ADVANCED MATERIALS INTERFACES
Open Access
www.advmatinterfaces.de

Chemiresistive Polymer Percolation Network Gas Sensor Created with a Nanosphere Template

Weishuo Li, Merel J. Lefferts, Yu Wang, Abigail M. Lister, Axel Forssberg, Runze Chen, Liren Wang, and Martin R. Castell**

The sensitivity and limits of detection (LOD) of chemiresistive gas sensors can often be improved by increasing the surface area of the sensing material that interacts with the analyte. This process is referred to as nanostructuring. Nanostructured polypyrrole (PPy) chemiresistive sensors for ammonia detection were created with the aid of a nanosphere template. Polystyrene nanospheres are deposited to form a template between interdigitated electrodes, and chronoamperometry is then used to grow PPy between the electrodes within the gaps of the nanospheres. The PPy growth is controlled to create electrical percolation networks. After removal of the nanospheres by dissolving them, the percolation behavior and sensing response of the nanostructured PPy sensors are investigated. The nanostructured percolation sensors show higher sensitivity and lower LOD to ammonia than percolation networks prepared without nanosphere templates. An optimal nanostructured ammonia percolation sensor with a chemiresistive sensitivity of $2.59 \pm 0.20\%$ ppm^{-1} and a LOD of 71 ± 6 ppb is obtained.

1. Introduction

Organic semiconductors have attracted broad academic and industrial interest owing to their flexibility, lightweight, ease of processing, and tunable properties.[1] They have great potential for use in a wide range of applications, such as for light emission,[2] as transistors,[3] as solar cells,[4] in electrochromism,[5] as supercapacitors,[6] and as sensors.[7] To create high-performance gas sensors using organic semiconductors, many different materials and device configurations have been explored. A variety of conducting polymers (CPs) have been used in different gas sensing devices including chemiresistors,[8] transistors,[9] and optical sensors.[10] Furthermore, molecular semiconductor–doped insulator heterojunctions based on small molecules have been designed to achieve stable gas detection.[11] Among various materials and device configurations, CP-based chemiresistors are regarded as one of the simplest methods of gas sensing.[12] CPs are deposited as a sensing layer during device fabrication, and interactions between the CPs and the analyte gas molecules cause changes in the electrical conductivity of the sensing layer that can be easily monitored.

Sensitivity is one of the most significant parameters for the sensing performance of chemiresistors and various approaches have to date been developed to improve it. Among all the reported approaches, nanostructuring is regarded as an effective strategy because morphologies with higher surface area-to-volume ratios can increase the sensitivity by improving the diffusion rate of gas molecules into and out of the CP-based sensing layers as well as providing more binding sites. To create nanostructured surfaces, CPs have in the past been fabricated through complex processes into different structures, including nanotubes, nanowires, nanoribbons, nanoparticles, and nanofibers.[13]

Electrical percolation is another effective approach to improve sensitivity.[14] For CP-based chemiresistors, electrical percolation is identified by the sharp increase in conductance between two electrodes during polymer deposition. In the percolation region, a relatively small number of electrical bridges are formed between the electrodes compared with a thin film. CP-based chemiresistors based on percolation networks are more sensitive compared to their thin-film counterparts. This is because the conductivity of an entire percolation pathway will be disrupted by the interaction of the analyte anywhere along the pathway, and this means that a small number of interactions between the analyte molecules and the CP percolation network will lead to a relatively large resistance change. On the other hand, for CP thin film sensors, the analyte only locally affects the surface conductivity of the thin film, resulting in lower sensitivity. Previous work has shown that electropolymerization can be used to fabricate chemiresistors based on polypyrrole (PPy) and poly(3,4-ethylenedioxythiophene) (PEDOT) percolation networks.[15] The sensitivities and limits of detection of the

W. Li, M. J. Lefferts, Y. Wang, A. M. Lister, A. Forssberg, R. Chen, L. Wang, M. R. Castell
Department of Materials
University of Oxford
Parks Road, Oxford OX1 3PH, UK
E-mail: weishuo.li@materials.ox.ac.uk; martin.castell@materials.ox.ac.uk

The ORCID identification number(s) for the author(s) of this article can be found under https://doi.org/10.1002/admi.202202042.

DOI: 10.1002/admi.202202042

resulting percolation networks to ammonia, nitrogen dioxide and ammonium nitrate/fuel oil are significantly improved compared to traditional thin-film chemiresistive sensors.

Because both nanostructuring and electrical percolation improve the sensitivity of CP-based chemiresistors, it is a natural step to combine these approaches. Here, electrochemical polymerisation to create percolation networks is coupled with nanosphere templating to facilitate nanostructuring. Nanosphere templating is an established, straightforward, cost-effective and reproducible technique for nanofabrication, which uses highly monodispersed nanospheres as deposition templates or etch masks for the fabrication of nanostructures.[16] It has previously been shown that electrochemical polymerisation can be performed between the nanospheres. After removal of the template, well-ordered CP networks with honeycomb-like or inverse-opal structures can be obtained and they can possess special surface and optical properties.[17] Owing to the unique properties of nanostructured polymers, electrochemical polymerisation coupled with nanosphere templating has been used in the creation of sensors, solar cells and other devices.[18]

In our work, nanosphere templating is used to create CP percolation networks with well-ordered nanostructures between interdigitated electrodes (IDEs). PPy is used to form the percolation networks because it can be grown straightforwardly using established electrochemical techniques [19] and it is known to change its electrical conductivity when exposed to ammonia gas.[7,20] We show that when nanostructured percolation networks are used in chemiresistive devices for the detection of ammonia they have higher sensitivities and lower LODs compared to their counterparts without nanosphere templates.

2. Result and Discussion

2.1. Preparation of Nanostructured Polypyrrole

Figure 1 shows a schematic of the preparation steps for the creation of the nanostructured PPy networks on platinum (Pt) IDEs.

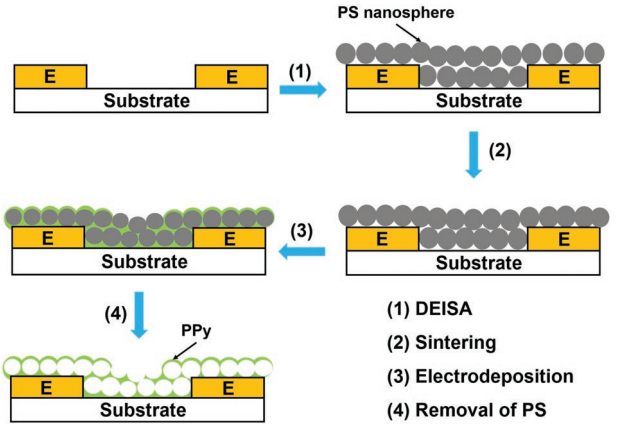

Figure 1. Schematic illustration of the preparation process of the nanostructured PPy sensor. Two electrodes (E) on a glass substrate are separated by a 5 µm gap. In Step 1 PS nanospheres are deposited onto the substrate. In Step 2 sintering is performed. In Step 3 PPy is grown electrochemically between the electrodes. In Step 4 the PS nanospheres are dissolved.

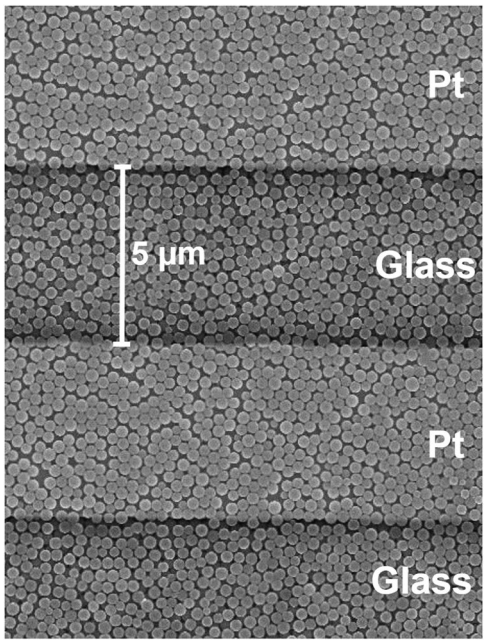

Figure 2. SEM image of a PS nanosphere template deposited on Pt IDEs. The PS nanospheres cover the electrodes and the gaps between the electrodes.

Monodispersed polystyrene (PS) nanospheres with a diameter of 300 nm were deposited on Pt IDEs via directed evaporation induced self-assembly (DEISA). The DEISA technique enables the creation of high-quality nanosphere templates to be deposited on substrates with controllable thickness and geometry.[22] The IDEs decorated with PS nanospheres were then placed on a heating plate at 90 °C for 1 h to induce moderate necking between the nanospheres. This sintering process is regarded as an effective way to improve the adhesion and stability of the nanosphere templates.[22–23] The scanning electron microscope (SEM) image in **Figure 2** shows the surface morphology of a nanosphere template on IDEs. The template exhibits a close-packed structure over most of the substrate.[24] Some narrow empty regions can be found between the close-packed domains. These are defects caused by the processes of DEISA and sintering. Using this method, a stable and well-ordered overlayer of PS nanospheres can be routinely obtained which is then used as a template for the electrochemical deposition of PPy.

PPy networks were grown on the PS nanosphere templates via chronoamperometry at 0.85 V. The electrochemical deposition process and electrolyte did not damage or alter the PS nanosphere templates. **Figure 3** shows an example of the current as a function of deposition time during chronoamperometry. Here the deposition current initially decreases from a relatively high value until approximately 10 s. This current decay could be attributed to a diffusion-controlled process involving the infiltration of pyrrole monomers to the Pt surface through the porous templates, or possibly an indication that the interaction with the bare Pt electrodes proceeds relatively rapidly until they are covered in polymer. When the current starts to increase after around 10 s, this indicates that the polymerisation of monomers and the doping process of the polymer starts to dominate the current. In the final processing step tetrahydrofuran (THF) is

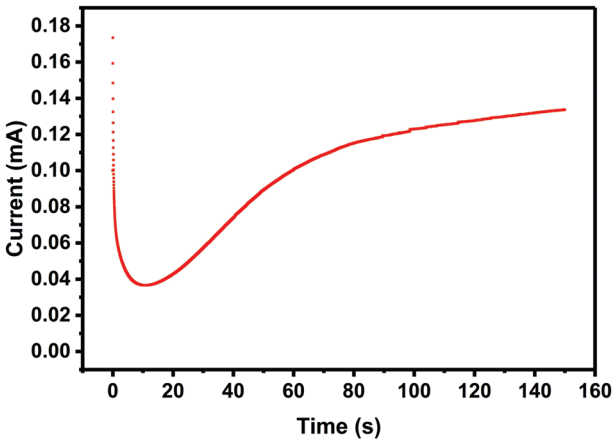

Figure 3. Chronoamperometric transient obtained for the deposition of PPy on the PS nanosphere template. The potential was set at 0.85 V and held for 150 s.

used to dissolve the PS nanospheres. The resulting deep blue PPy films are firmly attached to the IDEs without disintegrating during this process. Each sample exhibited similar electrical resistance values before and after nanosphere removal.

The chemical composition of PPy on the IDEs after nanosphere removal was determined by X-ray photoelectron spectroscopy (XPS) and Raman spectroscopy (**Figures 4** and **5**), and the results are consistent with those reported in the existing literature.[25] The XPS analysis (Figure 4) confirms the presence of p-doped PPy with ClO_4^- as the counterion. In the Raman spectrum (Figure 5), peaks attributed to polarons and bipolarons also support the formation of PPy in the p-doped state. No peaks related to PS (Figure S1, Supporting Information) were found, indicating the nanospheres on the surface of the sensing layers were fully removed through chemical etching.

2.2. Electrical Percolation

To study the electrical percolation behavior, various PPy networks were prepared on the PS nanosphere templates via chronoamperometry. Four repeat samples were obtained at a variety of deposition times ranging from 80 to 150 s. The resistance values between the IDE electrode fingers were recorded after the dissolution of the PS nanospheres (**Figure 6**). The linear plot in black shows the conductance ranging from the insulating region to the percolation region and then the thin-film region and is consistent with previously reported trends.[15a,21] The same data plotted as a semi-logarithmic plot in blue is used to determine the boundaries between insulating, percolation, and thin film regions. Initially, PPy nucleates and grows between PS nanospheres on the Pt IDE fingers. After filling the voids between the PS nanospheres on the IDE fingers, PPy starts to grow into the spaces between the nanospheres on the insulating gaps between the electrode fingers. No electrical conductance can be detected until 100 s of growth, indicating that samples prepared at 80 and 90 s belong to the insulating region. Then, from 100 s, the conductance sharply increases owing to the formation of PPy bridges between IDE fingers. This behavior demonstrates the percolation behavior

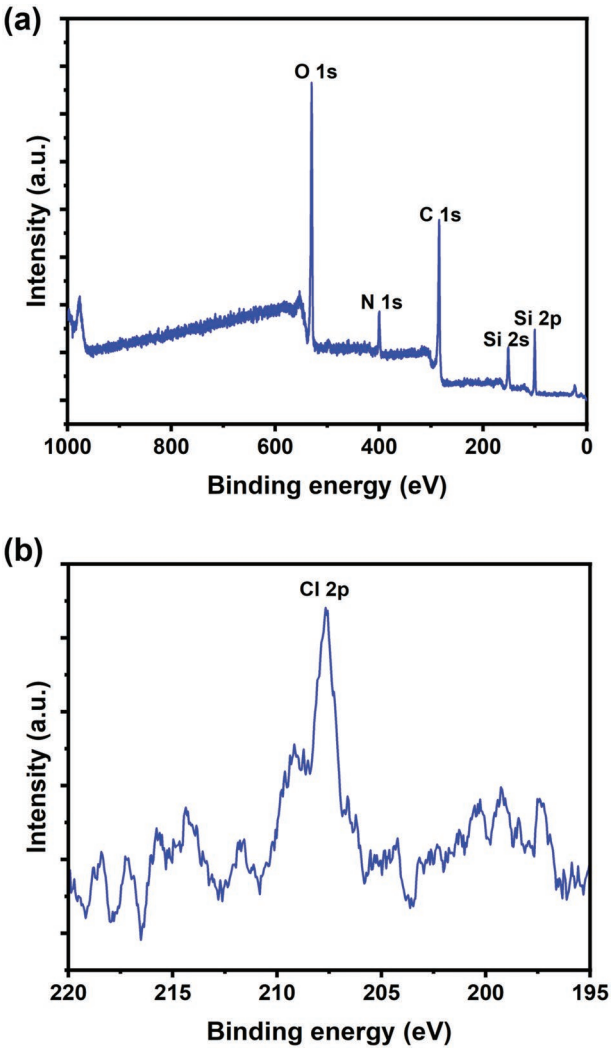

Figure 4. a) Survey-scan and b) Cl 2p XPS spectra of nanostructured PPy on the IDE after nanosphere removal. Si_{2s} and Si_{2p} signals originate from the glass substrate.

of PPy networks prepared with the PS nanosphere templates. As deposition proceeds, the fingers are fully connected and a PPy thin film is formed. Thus, the increase in conductance is less rapid at 140 s, indicating the end of the percolation region. It should be noted that variations in conductance for samples produced with identical procedures exist in both the percolation and the thin-film regions. This is attributed to several unavoidable factors including the variation between each template, the random nature of the polymer growth,[26] and the influence of the post-treatment washing procedure.

The SEM images in **Figure 7** show the growth of PPy networks on IDEs in a nanostructured form following the dissolution of the nanospheres. PPy networks consisting of bowl-shaped pores are obtained on Pt IDE fingers when the deposition process is stopped at 80 s (Figure 7a). At this early stage of growth, the thickness of this nanostructured PPy is thinner than that of the templates on the IDE fingers. As more PPy is deposited between the PS nanospheres, the pore size becomes smaller and PPy expands onto the glass gaps at 90 s

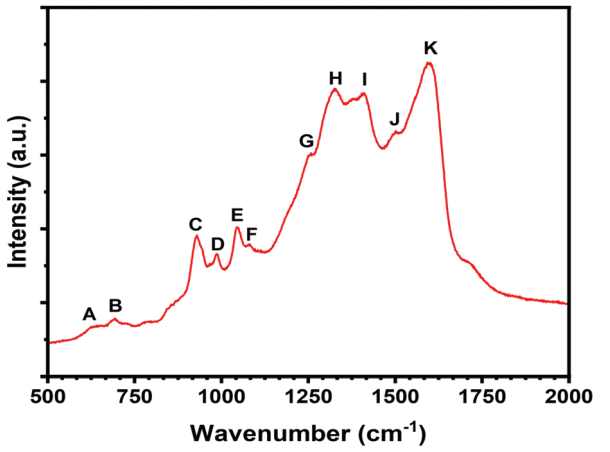

A: C–C ring torsional
B: C–H wagging
C: C–C ring deformation (bipolarons)
D: C–C ring deformation (polarons)
E: C–H in-plane deformation (polarons)
F: C–H in-plane deformation (bipolarons)
G: Antisymmetric C–H in-plane bending, ring stretching
H: C–C in-ring, antisymmetric C–N stretching
I: C–C in-ring, antisymmetric C–N stretching, C–H bending, N–H bending stretching
J: C–C, C=N stretching
K: C=C in-ring, C–C inter-ring stretching

Figure 5. Raman spectrum of nanostructured PPy on the IDE after nanosphere removal.

(Figure 7b). Shells in a close-packed structure can be observed on the fingers and even in some parts of the glass gaps from 100 s (Figure 7c–f). This suggests that the topmost layers of the templates in corresponding areas are fully covered with PPy at these stages. Otherwise, new layers of pores in a close-packed structure should appear in these areas after 100 s, changing the surface morphology of PPy networks. Figure 7c–f shows the increasing penetration of the PPy networks across the glass gaps. Although no obvious bridges are observed in Figure 7c,d, some conducting bridges must have formed at 100 s and 110 s

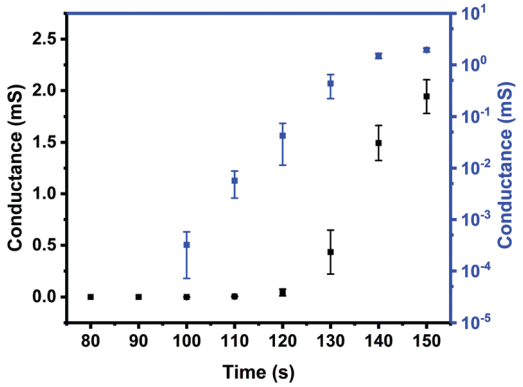

Figure 6. Plot of electrical conductance between the IDE electrodes versus deposition time in black, and the same data as a semi-logarithmic plot in blue for PPy deposition times of 80–150 s, measured after removal of the PS nanosphere templates. The error bars are the standard deviation of the conductance values of four separate samples.

based on the non-zero conductance measurements (Figure 6). The glass gaps are fully covered at 140 s, indicating that the electrical percolation regime ends at around 140 s (Figure 7g). This is consistent with the conductance measurements in Figure 6. From 140 s onwards, PPy networks close the upper layers in the middle of the gaps until a uniform overlayer is created (150 s, Figure 7h). Growth beyond 150 s adds to the thickness of the surface PPy film and is equivalent to a sensor in the thin-film region, where the increase in conductance slows down since film thickness becomes the major factor controlling film conductivity.

Although a porous bowl-shaped surface morphology is preferred due to its ability to absorb more chemicals to the interior of the polymer networks,[27] this remains challenging. The polymer growth starts on the IDE fingers and the growth on top of the fingers happens earlier than the growth across the glass gaps. Therefore, it is likely that the topmost layers of the templates in some areas are fully covered, leading to a structure of close-packed shells of PPy, before PPy bridges the gap between the electrodes. One possible solution would be to increase the thickness of the nanosphere templates.

2.3. Sensor Performance

Nanostructured PPy created with the PS nanosphere template was used to fabricate chemiresistors for gas sensing experiments. Percolation sensors called $S_{N\text{-}P1}$, $S_{N\text{-}P2}$, and $S_{N\text{-}P3}$ were fabricated by stopping electrochemical deposition at 130, 120, and 110 s, respectively. For performance comparison, a thin-film sensor called $S_{N\text{-}T}$ was fabricated at 140 s with the aid of the nanosphere template. The sensors were placed in our sensor testing chamber under N_2 flow and 1.0 V was applied across the IDEs. Sensors were then exposed to 1, 2, 3, and 4 parts per million (ppm) ammonia gas diluted with N_2, and the resulting change in resistance were recorded (**Figure 8**). As expected, the sensor resistance increases during the exposure to ammonia gas because electron-donating ammonia molecules reduce the number of hole charge carriers in p-doped PPy. The resistance decreases again when the sensor is left to recover under pure N_2. According to the published literature,[25b,d,28] the ammonia interaction mechanism with PPy occurs through electron transfer and/or proton transfer (**Scheme 1**). When interacting with NH_3 molecules, the p-doped PPy (PPy^+) is reduced to the neutral form (PPy^0) via a lone pair of electrons on the nitrogen atom of ammonia and/or the deprotonation of PPy creating ammonium salt ($NH_4^+X^-$). Figure 8 shows that higher ammonia concentrations result in larger resistance changes and sensors with higher initial resistances exhibit higher levels of noise. This is in agreement with our previous work.[15a,21] It should be noted that the resistance change during the first exposure to 4 ppm ammonia is greater than those for subsequent exposures. This feature suggests that the interaction of nanostructured PPy networks with ammonia is not fully reversible on the time scale of these experiments. A longer recovery time of 2 h improves the reversibility at 4 ppm (Figure S2, Supporting Information). Similar to the reported work,[29] our sensors can also recover to the baseline values by annealing at 100 °C. After the first exposure better reversibility of the resistance change is seen for each sensor within 15 min of recovery.

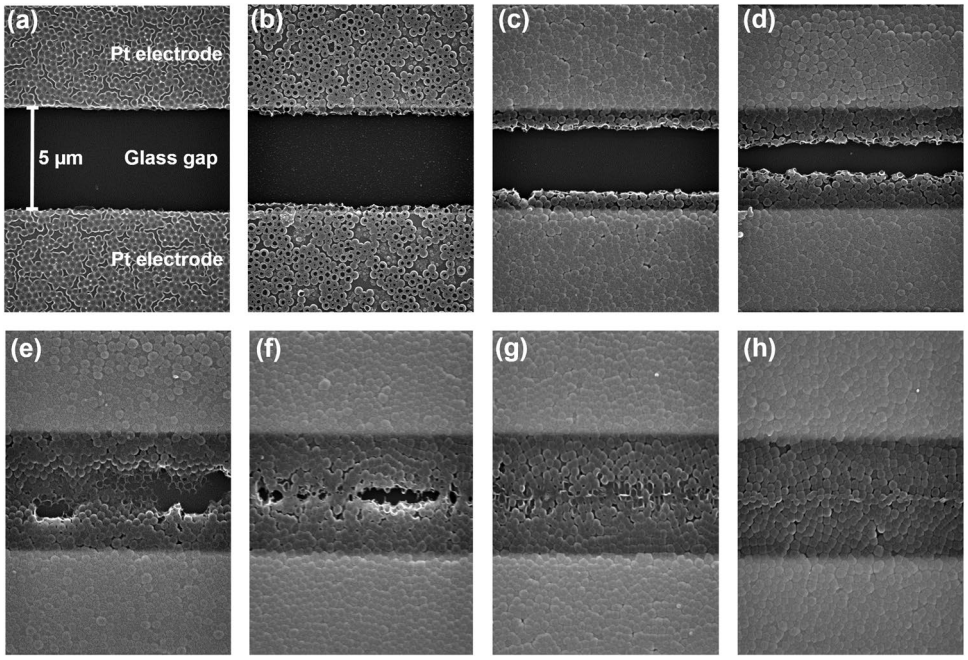

Figure 7. SEM images of nanostructured PPy prepared with the PS nanosphere templates via chronoamperometry on Pt IDEs for a) 80, b) 90, c) 100, d) 110, e) 120, f) 130, g), 140, and (h) 150 s. As the deposition time increases, both the amount of PPy on the Pt fingers (light grey) and across the glass gaps (dark grey) increases.

With better reversibility of the resistance change than the first exposure, the subsequent exposures for each sensor were used for further sensor evaluation and analysis. The sensing responses of $S_{N\text{-}T}$, $S_{N\text{-}P1}$, $S_{N\text{-}P2}$, and $S_{N\text{-}P3}$ were obtained by calculating the percentage change relative to the starting resistances before exposure ($\Delta R/R_0 \times 100\%$). For each sensor, a linear relationship was observed between the sensing response and the concentration of ammonia (**Figure 9**). The sensitivity is defined as the slope of the linear fit in Figure 9 and the limit of detection (LOD) is defined as three times the standard deviation of the baseline noise level (σ) divided by the sensitivity. **Figure 10** shows that $S_{N\text{-}T}$, obtained in the thin film-region, exhibits low sensitivity. As the initial resistance increases, the sensitivity also increases and becomes stable above 2.5% ppm^{-1}, where electrical percolation determines the sensitivity. In the percolation region, interactions between PPy networks and ammonia molecules have a larger effect on the resistance of the networks, resulting in a significantly increased sensitivity compared to thin film-based sensors. As shown in Figure 8, higher initial resistances also lead to higher levels of noise. Therefore, the LOD first decreases and then increases since it is determined by a competitive relationship between sensitivity and baseline noise, which is in agreement with our previous work for PPy percolation networks without the nanosphere templates.[15a,21] Especially for the sensor $S_{N\text{-}P3}$, its high level of noise results in a very high LOD around 1 ppm, which is consistent with the result in Figure 8d. Among these sensors based on nanostructured PPy networks, $S_{N\text{-}P1}$ is regarded as the optimal sensor with a sensitivity of $2.59 \pm 0.20\%$ ppm^{-1} and a LOD of 71 ± 6 ppb.

For comparison, a series of sensors called $S_{B\text{-}T}$, $S_{B\text{-}P1}$, $S_{B\text{-}P2}$, and $S_{B\text{-}P3}$ were fabricated on Pt IDEs without nanosphere templates (Figure S3, Supporting Information). For each blank sample, its sensing responses were obtained using the same method for sensing experiments, and a linear relationship was also observed between the sensing response and the concentration of ammonia (Figures S4 and S5, Supporting Information). As shown in Figure 10, these sensors exhibit similar trends in sensitivity and LOD to those based on nanostructured PPy. However, their nanostructured counterparts show higher sensitivities in the percolation region because the introduction of nanostructuring provides higher surface area-to-volume ratios. This indicates that creating nanostructured CP networks with nanosphere templates is a promising approach to further improve the sensing performances of the polymer percolation sensors.

Although a systematic comparison between each sensor can be difficult to accomplish since experimental conditions like temperature, response time, and analyte flow rate may vary, attempts have been made to compare the optimal sensor in this work ($S_{N\text{-}P1}$) with other PPy-based chemiresistors from previous studies (Table S1, Supporting Information). As far as we know, only a few sensors exhibit high sensitivities above 2% ppm^{-1} with detection ranges under 10 ppm (**Figure 11**).[13c,i,15a,21,30] This indicates that $S_{N\text{-}P1}$ prepared with the nanosphere template shows a desirable sensitivity of $2.59 \pm 0.20\%$ ppm^{-1} at low concentrations. Moreover, its LOD of 71 ± 6 ppb demonstrates the ability to detect ammonia under 100 ppb, which is competitive with other PPy-based chemiresistors.[13h,31] Combining the benefits of nanostructuring and electrical percolation, creating nanostructured CP networks with nanosphere templates is a promising method to fabricate PPy-based sensors with enhanced performance. To further improve sensor performance, many factors should be considered in future work, such

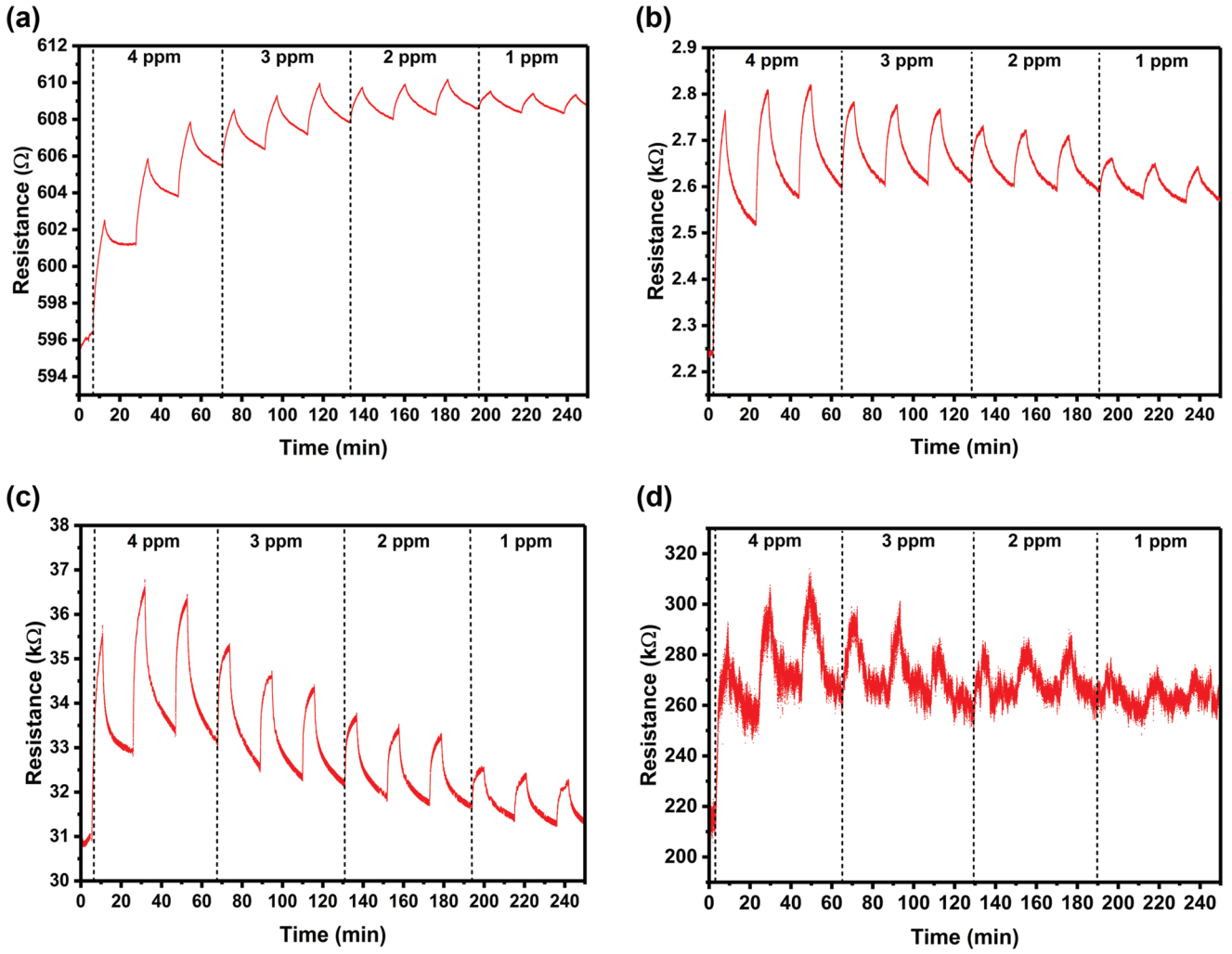

Figure 8. Sensor response to ammonia for the chemiresistors a) $S_{N\text{-}T}$, b) $S_{N\text{-}P1}$, c) $S_{N\text{-}P2}$, and d) $S_{N\text{-}P3}$ based on nanostructured PPy at deposition times of 140, 130, 120, and 110 s, respectively. $S_{N\text{-}T}$ was obtained in the thin-film region while $S_{N\text{-}P1}$, $S_{N\text{-}P2}$, and $S_{N\text{-}P3}$ were obtained in the percolation region. All sensors were exposed three times to 1, 2, 3, and 4 ppm NH_3 in N_2 for 6 min, with a 15 min recovery time under pure N_2 flow between exposures. The subscript N-T means nanostructured PPy in the thin film region and N-P means nanostructured PPy in the percolation region. The test temperature is 26 ± 1 °C and the humidity is 1.22 ± 0.23% RH.

as the material porosity,[32] the deposition potential, and the type of the counterion.[30,33]

Figure 11 also shows that sensors with different performances are applicable in different fields of ammonia detection, spanning from industrial and daily safety (>25 ppm) to medical diagnosis (0.4–14.7 ppm).[13h,34] With a high sensitivity at low concentrations, $S_{N\text{-}P1}$ shows its potential in point-of-care applications for medical diagnosis. Analyzing its responses to ammonia gas from human breath could be a promising approach to the early detection of many diseases, such as ulcers, hepatic injury, renal disorders, and cancers.[28a,29,30] Compared with instrument-based testing, a non-invasive device has various advantages including low cost, no requirement for experienced operators, time saving, and low power consumption.[35]

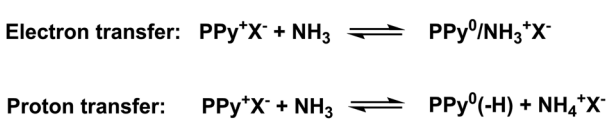

Scheme 1. Detection mechanisms of PPy towards ammonia. (X^-: counterion).

To further characterize the optimal sensor ($S_{N\text{-}P1}$) in this work, more sensors based on nanostructured percolation PPy were reproduced at the deposition time of 130 s, and additional performance parameters including selectivity, stability, and the influence of humidity were investigated. Figure S6a (Supporting Information) shows the selectivity of ammonia compared with other toxic gases such as CO and NO_2. This can be attributed to the different electron-donating and withdrawing properties of the different analytes. Probably due to the film aging and/or the reduction in the number of unstable adsorption sites,[13j,36] a slow decay of the sensing response was observed during a 2-week study (Figure S6b, Supporting Information). Furthermore, as the relative humidity increases up to 20% RH (Figure S6c, Supporting Information), the sensing response to ammonia drops because the proton transfer

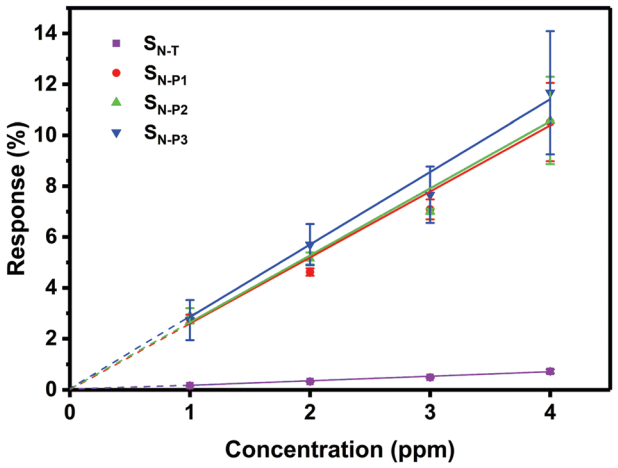

Figure 9. Sensing responses ($\Delta R/R_0 \times 100\%$) as a function of ammonia concentration for S_{N-T}, S_{N-P1}, S_{N-P2}, and S_{N-P3}.

induced by water molecules reduces the number of the sensing sites for ammonia molecules.[37]

3. Conclusion

Nanostructured PPy-based chemiresistors were fabricated with nanosphere templates via electrochemical polymerization. During preparation PS nanosphere templates were created via directed evaporation induced self-assembly and PPy networks were obtained via chronoamperometry on the nanosphere templates. After the dissolution of the nanosphere templates, this resulted in nanostructured PPy layers, whose composition was confirmed by XPS and Raman spectroscopy. By varying the electrochemical deposition time PPy layer densities spanning from the insulating region to the thin-film region were

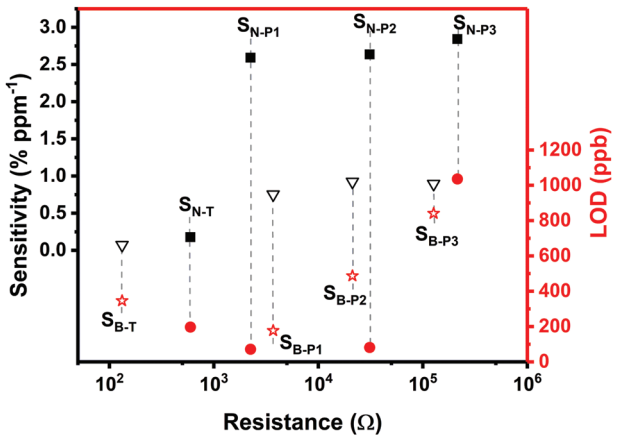

Figure 10. Values of sensitivity (black data points) and LOD (red data points) for the sensors investigated. Black-filled squares are the sensitivities of the nanostructured sensors, and red-filled points are the corresponding LODs. Blank samples for comparison (black open triangles and red open stars), S_{B-T}, S_{B-P1}, S_{B-P2}, and S_{B-P3} were fabricated on blank Pt IDEs without PS nanosphere templates. S_{B-T} was obtained in the thin-film region while S_{B-P1}, S_{B-P2}, and S_{B-P3} were obtained in the percolation region. The dashed lines connect the sensitivity and LOD for each sensor.

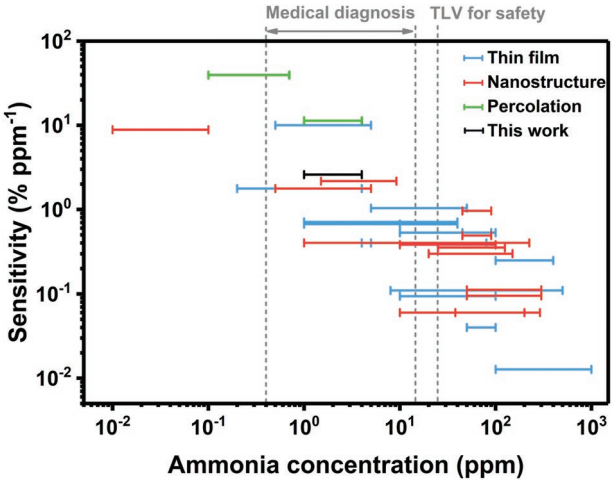

Figure 11. Sensitivities and corresponding detection ranges during sensing experiments for S_{N-P1} (in black) and other PPy-based chemiresistors from previous studies. Sensors from previous studies have been classified according to Table S1, Supporting Information, including thin-film sensors (in blue), sensors based on nanostructured PPy (in red), and percolation sensors (in green). Most of the sensors show desirable detection ranges covering the threshold limit value of 25 ppm for industrial and daily safety. Sensors with detection ranges at low concentrations (0.4–14.7 ppm) are applicable for medical diagnosis.

obtained. The electrical percolation behavior of the nanostructured PPy networks was confirmed by electrical measurements and SEM imaging. The sensing responses to the ammonia of nanostructured PPy layers fabricated by this method in both the thin-film and percolation regions were investigated. Compared with their counterparts prepared on IDEs without templates, they show better sensing performances to ammonia, indicating that creating nanostructured CP networks with nanosphere templates is a promising approach to further improve the performances of percolation sensors. An optimal sensor (S_{N-P1}) with a sensitivity of 2.59 ± 0.20% ppm^{-1} and a LOD of 71 ± 6 ppb was obtained and it has a competitive performance when compared with other PPy-based chemiresistors for ammonia detection. With a desirable sensitivity at low concentrations, our optimal sensor has potential in point-of-care applications.

4. Experimental Section

Preparation of Nanosphere Templates: All the chemicals for template preparation were purchased from Sigma–Aldrich (UK). Pt interdigitated electrodes (IDEs) were purchased from Micrux (Spain). Each IDE consists of 180 pairs of 5 µm wide Pt electrodes separated by a gap of 5 µm on an insulating glass substrate. Prior to use, each substrate was treated with piranha solution (H_2SO_4:30% H_2O_2 = 3:1, by volume; warning: piranha solution is very corrosive and must be treated with extreme care) at 50 °C for 30 min to enhance its hydrophilic nature and then washed carefully with de-ionized water and ethanol (C_2H_5OH, 99.8%). The nanosphere templates were prepared via directed evaporation induced self-assembly (DEISA). During this process, substrates were vertically immersed in a 50 mL glass beaker containing 10 mL of ethanol (C_2H_5OH, 99.8%) and 20 µL of 10 wt% latex of polystyrene (PS) nanospheres in water. The mean diameter of the PS

nanospheres is 300 nm. The beaker was then left at room temperature for 60 h until all the solvents had evaporated. After DEISA, the substrates decorated with PS nanospheres were sintered at 90 °C for 1 h.

Electropolymerization of Polypyrrole: All the chemicals for PPy preparation were purchased from Sigma–Aldrich (UK). Electrochemical deposition was performed using a PGSTAT204 Autolab electrochemical workstation (Eco Chemie, Netherlands) interfaced to a PC with NOVA version 2.1 software. The three-electrode cell used a Pt coil (BASi, USA) as the counter electrode, an Ag/AgCl (CH Instruments, USA) reference electrode, and the Pt IDEs of the sample with a previous deposited nanosphere template as the working electrode. PPy was synthesized by chronoamperometry at 0.85 V from a solution of 10 mM pyrrole (Py, 98%) and 0.1 M lithium perchlorate ($LiClO_4$, 95%) in de-ionized water. Samples with various polymer coverages were prepared by halting electropolymerization at different deposition times. After deposition, samples were carefully washed with acetonitrile (CH_3CN, 99%) and dried in air for 10 min. The PS nanospheres were removed by immersing the samples in a tetrahydrofuran (THF) bath for 24 h followed by a THF rinse. After the removal of PS the samples were dried under ambient conditions.

Characterization: The surface morphologies of the nanosphere templates and PPy networks were imaged using a Zeiss Merlin scanning electron microscope (SEM) at an accelerating voltage of 10 kV. The surface composition of PPy on the IDEs was determined using a PHI VersaProbe III X-ray photoelectron spectrometer (XPS) with monochromated Al Kα X-ray radiation (1486.6 eV), a 5 µm beam, and an analyzer pass energy of 224 eV with 0.28 eV energy resolution. XPS data were processed with smoothing, using a moving average of 15 points. To further confirm the chemical composition of PPy on the IDEs, Raman analysis was carried out using a Renishaw InVia Raman microscope employing a 633 nm laser. The acquisition time was set to 10 s, while five repetitions were acquired to improve the signal/noise ratio. The resistance of each sensor was measured using an RS PRO IDM 98IV handheld digital multimeter.

Sensing Experiments: Sensing experiments were carried out in a custom-made sensing chamber at room temperature under atmospheric pressure.[21] Ammonia gas (10 ppm, nitrogen fill) and nitrogen gas (for further dilution of the ammonia) were purchased from BOC gases UK. The flow rate from each gas cylinder was controlled by a mass flow controller (Alicat) and the concentration of ammonia gas was determined by the relative flow rates of the two mass flow controllers. Gases were mixed at a T-joint before entering the gas inlet of the chamber and a constant total flow rate was maintained at 500 standard cubic centimeters per minute (sccm) throughout the experiments. Each sensor was placed in the chamber and connected to a B2900A source/measure unit (Keysight, UK). The chamber was first purged with nitrogen gas for 30 min to remove impurities from the chamber and the sensing layer. Then, a dc potential of 1.0 V was applied across the two interdigitated electrodes of the sensor and the current was monitored on a PC equipped with Benchvue software. Once a stable current baseline was reached, the sensor was exposed to concentrations of ammonia gas from 1 to 4 parts per million (ppm) for 6 min each. After each exposure, the sensor was purged with nitrogen for 15 min before the next exposure.

Supporting Information

Supporting Information is available from the Wiley Online Library or from the author.

Acknowledgements

The authors are grateful for support from the EPSRC via the WAFT collaboration (EP/M015173/1) and the Global Challenges Research Fund (GCRF).

Conflict of Interest

The authors declare no conflict of interest.

Data Availability Statement

The data that support the findings of this study are available from the corresponding author upon reasonable request.

Keywords

conducting polymer, electrochemical polymerisation, gas sensor, nanostructuring, percolation network

Received: September 14, 2022
Revised: November 23, 2022
Published online:

[1] a) S. Riera-Galindo, F. Leonardi, R. Pfattner, M. Mas-Torrent, *Adv. Mater.* **2019**, *4*, 1900104; b) Y. Han, L. Bai, J. Lin, X. Ding, L. Xie, W. Huang, *Adv. Funct. Mater.* **2021**, *31*, 2105092.
[2] A. Salehi, X. Fu, D.-H. Shin, F. So, *Adv. Funct. Mater.* **2019**, *29*, 1808803.
[3] H. Matsui, Y. Takeda, S. Tokito, *Org. Electron.* **2019**, *75*, 105432.
[4] L. Dou, J. You, Z. Hong, Z. Xu, G. Li, R. A. Street, Y. Yang, *Adv. Mater.* **2013**, *25*, 6642.
[5] W. S. Li, Y. T. Guo, J. J. Shi, H. T. Yu, H. Meng, *Macromolecules* **2016**, *49*, 7211.
[6] W. Li, Y. Guo, Y. Wang, X. Xing, X. Chen, J. Ning, H. Yu, Y. Shi, I. Murtaza, H. Meng, *J. Mater. Chem.* **2019**, *7*, 116.
[7] Y. C. Wong, B. C. Ang, A. Haseeb, A. A. Baharuddin, Y. H. Wong, *J. Electrochem. Soc.* **2019**, *167*, 037503.
[8] C. Zhu, X. Dong, C. Guo, L. Huo, S. Gao, Z. Zheng, X. Cheng, Y. Xu, *J. Mater. Chem. A* **2022**, *10*, 12150.
[9] S. H. Yu, H. G. Girma, K. M. Sim, S. Yoon, J. M. Park, H. Kong, D. S. Chung, *Nanoscale* **2019**, *11*, 17709.
[10] Y. S. Chiam, K. S. Lim, S. W. Harun, S. N. Gan, S. W. Phang, *Sen. Actuators, A* **2014**, *205*, 58.
[11] a) M. Bouvet, V. Parra, U.S. 8450725, **2013**; b) A. Wannebroucq, G. Gruntz, J.-M. Suisse, Y. Nicolas, R. Meunier-Prest, M. Mateos, T. Toupance, M. Bouvet, *Sens. Actuators, B: Chem.* **2018**, *255*, 1694.
[12] H. Bai, G. Shi, *Sensors* **2007**, *7*, 267.
[13] a) H. Yoon, M. Chang, J. Jang, *J. Phys. Chem. B* **2006**, *110*, 14074; b) S. C. Hernandez, D. Chaudhuri, W. Chen, N. V. Myung, A. Mulchandani, *Electroanalysis* **2007**, *19*, 2125; c) L. Zhang, F. Meng, Y. Chen, J. Liu, Y. Sun, T. Luo, M. Li, J. Liu, *Sens. Actuators, B: Chem.* **2009**, *142*, 204; d) N. Chartuprayoon, C. M. Hangarter, Y. Rheem, H. Jung, N. V. Myung, *J. Phys. Chem. C* **2010**, *114*, 11103; e) O. S. Kwon, J.-Y. Hong, S. J. Park, Y. Jang, J. Jang, *J. Phys. Chem. C* **2010**, *114*, 18874; f) Ishpal, A. Kaur, *J. Nanopart. Res.* **2013**, *15*, 1637; g) H.-A. Kalaleh, K. Masri, *J. Mater. Sci.: Mater. Electron.* **2021**, *32*, 5978; h) H. T. Hien, C. Van Tuan, D. T. Anh Thu, P. Q. Ngan, G. H. Thai, S. C. Doanh, H. T. Giang, N. D. Van, T. Trung, *Synth. Met.* **2019**, *250*, 35; i) J. S. Lee, J. Jun, D. H. Shin, J. Jang, *Nanoscale* **2014**, *6*, 4188; j) C. She, G. Li, W. Zhang, G. Xie, Y. Zhang, L. Li, F. Yue, S. Liu, C. Jing, Y. Cheng, J. Chu, *Sens. Actuators, A* **2021**, *317*, 112436; k) X. Yang, L. Li, *Synth. Met.* **2010**, *160*, 1365.
[14] a) T. Sauerwald, S. Russ, in *Gas Sensing Fundamentals*, (Eds: C.-D. Kohl, T. Wagner), Springer Berlin Heidelberg, Berlin, Heidelberg **2014**, Chapter p. 53; b) L. Hu, D. Hecht, G. Grüner,

Nano Lett. **2004**, *4*, 2513; c) J. Gao, H. Wang, X. Huang, M. Hu, H. Xue, R. K. Y. Li, *Compos. Sci. Technol.* **2018**, *161*, 135.

[15] a) B. I. Armitage, K. Murugappan, M. J. Lefferts, A. Cowsik, M. R. Castell, *J. Mater. Chem. C* **2020**, *8*, 12669; b) M. J. Lefferts, B. I. Armitage, K. Murugappan, M. R. Castell, *RSC Adv.* **2021**, *11*, 22789; c) M. J. Lefferts, L. H. Humphreys, N. Mai, K. Murugappan, B. I. Armitage, J.-F. Pons, M. R. Castell, *Analyst* **2021**, *146*, 2186; d) M. J. Lefferts, K. Murugappan, C. Wu, M. R. Castell, *Appl. Phys. Lett.* **2018**, *112*, 251602; e) K. Murugappan, M. R. Castell, *Electrochem. Commun.* **2018**, *87*, 40.

[16] J. Li, Y. Hu, L. Yu, L. Li, D. Ji, L. Li, W. Hu, H. Fuchs, *Small* **2021**, *17*, 2100724.

[17] a) V.-Q. Nguyen, D. Schaming, P. Martin, J.-C. Lacroix, *ACS Appl. Mater. Interfaces* **2015**, *7*, 21673; b) D. P. Puzzo, A. C. Arsenault, I. Manners, G. A. Ozin, *Angew. Chem., Int. Ed.* **2009**, *48*, 943.

[18] a) T. Cassagneau, F. Caruso, *Adv. Mater.* **2002**, *14*, 1837; b) L. Zhao, L. Tong, C. Li, Z. Gu, G. Shi, *J. Mater. Chem.* **2009**, *19*, 1653; c) Q. Zhong, H. Xu, H. Ding, L. Bai, Z. Mu, Z. Xie, Y. Zhao, Z. Gu, *Colloids Surf. Physicochem. Eng. Aspects* **2013**, *433*, 59; d) A. Cernat, A. L.e Goff, M. Holzinger, R. Sandulescu, S. Cosnier, *Anal. Bioanal. Chem.* **2014**, *406*, 1141; e) S. H. Park, O.-H. Kim, J. S. Kang, K. J. Lee, J.-W. Choi, Y.-H. Cho, Y.-E. Sung, *Electrochim. Acta* **2014**, *137*, 661; f) J. Szűcs, T. Lindfors, J. Bobacka, R. E. Gyurcsányi, *Electroanalysis* **2016**, *28*, 778; g) P. Wu, J. Guo, K. Jiang, J. Wang, L. Jiang, *Adv. Funct. Mater.* **2019**, *29*, 1808473.

[19] a) M. Das, S. Roy, *Mater. Sci. Semicond. Process.* **2021**, *121*, 105332; b) M. R. Miah, M. Yang, S. Khandaker, M. M. Bashar, A. K. D. Alsukaibi, H. M. A. Hassan, H. Znad, M. R. Awual, *Sens. Actuators, A* **2022**, *347*, 113933.

[20] D. Kwak, Y. Lei, R. Maric, *Talanta* **2019**, *204*, 713.

[21] W. Li, M. J. Lefferts, B. I. Armitage, K. Murugappan, M. R. Castell, *ACS Appl. Polym. Mater.* **2022**, *4*, 2536.

[22] R. W. J. Scott, S. M. Yang, D. E. Williams, G. A. Ozin, *Chem. Commun.* **2003**, 688.

[23] J. H. Pikul, S. Özerinç, B. Liu, R. Zhang, P. V. Braun, V. S. Deshpande, W. P. King, *Sci. Rep.* **2019**, *9*, 719.

[24] X. Yang, Y. Jin, Y. Zhu, L. Tang, C. Li, *J. Electrochem. Soc.* **2008**, *155*, J23.

[25] a) S. Carquigny, J.-B. Sanchez, F. Berger, B. Lakard, F. Lallemand, *Talanta* **2009**, *78*, 199; b) M. Šetka, R. Calavia, L. Vojkůvka, E. Llobet, J. Drbohlavová, S. Vallejos, *Sci. Rep.* **2019**, *9*, 8465; c) M. Šetka, R. Calavia, L. Vojkůvka, J. Polčák, E. Llobet, D. Jana, S. Vallejos, *Mater. Today Proc.* **2020**, *20*, 305; d) J. Casanova-Chafer, P. Umek, S. Acosta, C. Bittencourt, E. Llobet, *ACS Appl. Mater. Interfaces* **2021**, *13*, 40909.

[26] a) D.-H. Han, J.-W. Kim, S.-M. Park, *J. Phys. Chem. B* **2006**, *110*, 14874; b) J. A. Del-Oso, B. A. Frontana-Uribe, J.-L. Maldonado, M. Rivera, M. Tapia-Tapia, G. Roa-Morales, *J. Solid State Electrochem.* **2018**, *22*, 2025.

[27] S. Tian, J. Wang, U. Jonas, W. Knoll, *Chem. Mater.* **2005**, *17*, 5726.

[28] a) M. Salimi, F. Rahmani, S. M. R. M. Hosseini, *ChemistrySelect* **2021**, *6*, 7829; b) M. Šetka, J. Drbohlavová, J. Hubálek, *Sensors* **2017**, *17*, 562.

[29] X. Tang, J.-P. Raskin, N. Kryvutsa, S. Hermans, O. Slobodian, A. N. Nazarov, M. Debliquy, *Sens. Actuators, B: Chem.* **2020**, *305*, 127423.

[30] A. Ly, Y. Luo, G. Cavaillès, M.-G. Olivier, M. Debliquy, D. Lahem, *Chemosensors* **2020**, *8*, 38.

[31] S. Majumdar, K. Sarmah, D. Mahanta, *ACS Appl. Polym. Mater.* **2020**, *2*, 1933.

[32] Y. Hong, V. Rozyyev, C. T. Yavuz, *Small Sci.* **2021**, *1*, 2000078.

[33] A. Amini, A. Jafari, M. Vafaei, M. Mahmoodian, *J. Mater. Sci.: Mater. Electron.* **2022**, *33*, 1293.

[34] a) K. Wetchakun, T. Samerjai, N. Tamaekong, C. Liewhiran, C. Siriwong, V. Kruefu, A. Wisitsoraat, A. Tuantranont, S. Phanichphant, *Sens. Actuators, B: Chem.* **2011**, *160*, 580; b) M. Gafare, J. O. Dennis, M. H. D. Khir, *Int. j. innov. res. appl. sci. eng.* **2014**, *1621*, 303; c) I.-A. Pavel, S. Lakard, B. Lakard, *Chemosensors* **2022**, *10*, 97; d) S. Wang, Y. Jiang, B. Liu, Z. Duan, H. Pan, Z. Yuan, G. Xie, J. Wang, Z. Fang, H. Tai, *Sens. Actuators, B: Chem.* **2021**, *343*, 130069.

[35] I. C. Weber, N. Derron, K. Königstein, P. A. Gerber, A. T. Güntner, S. E. Pratsinis, *Small Sci.* **2021**, *1*, 2100004.

[36] S. T. Navale, A. T. Mane, M. A. Chougule, R. D. Sakhare, S. R. Nalage, V. B. Patil, *Synth. Met.* **2014**, *189*, 94.

[37] a) W. Geng, N. Li, X. Li, R. Wang, J. Tu, T. Zhang, *Sens. Actuators, B: Chem.* **2007**, *125*, 114; b) M. Joulazadeh, A. H. Navarchian, M. Niroomand, *Adv. Polym. Technol.* **2014**, 33.